Eur J Nucl Med Mol Imaging (2010) 37:920–933
DOI 10.1007/s00259-009-1340-5

ORIGINAL ARTICLE

Kinetic analysis of the cannabinoid-1 receptor PET tracer [^{18}F]MK-9470 in human brain

Sandra Marina Sanabria-Bohórquez · Terence G. Hamill · Karolien Goffin · Inge De Lepeleire · Guy Bormans · H. Donald Burns · Koen Van Laere

Received: 10 August 2009 / Accepted: 13 November 2009 / Published online: 24 December 2009
© Springer-Verlag 2009

Abstract
Purpose Quantitative imaging of the type 1 cannabinoid receptor (CB1R) opens perspectives for many neurological and psychiatric disorders. We characterized the kinetics and reproducibility of the CB1R tracer [^{18}F]MK-9470 in human brain.
Methods [^{18}F]MK-9470 data were analysed using reversible models and the distribution volume V_T and $V_{ND}k_3$ ($V_{ND}k_3 = K_1k_2$) were estimated. Tracer binding was also evaluated using irreversible kinetics and the irreversible uptake constant K_i and fractional uptake rate (FUR) were estimated. The effect of blood flow on these parameters was evaluated. Additionally, the possibility of determining the tracer plasma kinetics using a reduced number of blood samples was also examined.
Results A reversible two-tissue compartment model using a global k_4 value was necessary to describe brain kinetics. Both V_T and $V_{ND}k_3$ were estimated satisfactorily and their test–retest variability was between 10% and 30%. Irreversible methods adequately described brain kinetics and FUR values were equivalent to K_i. The linear relationship between K_i and $V_{ND}k_3$ demonstrated that K_i or FUR and thus the simple measure of tracer brain uptake provide CB1R availability information. The test–retest variability of K_i and FUR was <10% and estimates were independent of blood flow. Brain uptake can be used as a receptor availability index, albeit at the expense of potential bias due to between-subject differences in tracer plasma kinetics.
Conclusion [^{18}F]MK-9470 specific binding can be accurately determined using FUR values requiring a short scan 90 to 120 min after tracer administration. Our results suggest that [^{18}F]MK-9470 plasma kinetics can be assessed using a few venous samples.

Keywords [^{18}F]MK-9470 · Human brain · CB1 receptor · Kinetic modelling

S. M. Sanabria-Bohórquez (✉) · T. G. Hamill · H. D. Burns
Imaging, Merck Research Laboratories,
Sumneytown Pike WP44D-2,
West Point, PA 19486, USA
e-mail: sandra_sanabria@merck.com

K. Goffin · K. Van Laere
Division of Nuclear Medicine, University Hospital and K.U. Leuven,
Leuven, Belgium

I. De Lepeleire
Merck Research Laboratories,
Brussels, Belgium

G. Bormans
Laboratory of Radiopharmacy, K.U.Leuven,
Leuven, Belgium

Introduction

The pharmacological effects of tetrahydrocannabinol (Δ^9-THC), the major constituent of marijuana, and other exogenous and endogenous cannabinoids are known to be mediated through specific G-protein-coupled receptors [1, 2]. Type 1 cannabinoid receptors (CB1R) are predominantly located in the central nervous system and are one of the most abundantly expressed G-protein-coupled receptors known with a level of expression up to 1 pmol/mg tissue or greater [3]. The CB1R plays an important role in short- and long-term control of synaptic transmission and is predominantly presynaptically located with a main inhibitory effect on transmitter release [4]. The CB1R is involved in cognition, especially learning and memory, as well as in motor

behaviour, pain and weight control. Pharmacological manipulation of the CB1R is a promising approach as an adjuvant therapeutic intervention for several neuropsychiatric disorders [5]. For example, selective CB1 inverse agonists reduce appetite, and weight loss has been observed during long-term administration [6], probably due to a combination of central and peripheral effects [7].

To understand the (patho)physiological and pharmacological role played by the CB1R, in vivo binding data in the human brain are required. There are significant differences in the regional distribution of CB1R, mRNA and signal transduction coupling between mammalian species [8, 9]. Moreover, differences in detection of CB1R with various classes of antibodies have been found [10], and difficulties with interpretation and methodological variables may confound post-mortem research.

Recently, new radioligands with improved imaging characteristics have been developed that enable visualization of the CB1R using PET [11]. The PET tracer, [^{18}F]MK-9470 or *N*-[2-(3-cyano-phenyl)-3-(4-(2-^{18}F-fluoroethoxy)phenyl)-1-methylpropyl]-2-(5-methyl-2-pyridyloxy)-2-methylproponamide (Merck Research Laboratories, West Point, PA) [12], is an inverse agonist with high selectivity and specificity for the human CB1R [13, 14]. [^{18}F]MK-9470 has been used to support CB1R inverse agonist drug development in preclinical and clinical settings for measuring receptor occupancy [7, 13], as well as for investigating CB1R changes with normal ageing [15].

The main goal of this work was to characterize the kinetics of [^{18}F]MK-9470 in the human brain. Although, the reversibility of [^{18}F]MK-9470 is difficult to assess directly in human subjects because high CB1R occupancy or "chase" studies are not feasible due to the undesirable side effects of high doses of antagonist or inverse agonist compounds, preclinical studies in nonhuman primates have demonstrated that the tracer binds reversibly to CB1R [13]. However, given the slow kinetics of the tracer, we evaluated the [^{18}F]MK-9470 human data using both reversible and irreversible tracer kinetic modelling and developed a suitable and reliable method of analysis for accurate CB1R quantification. The suitability of the irreversible tracer kinetic parameters to provide CB1R availability information was assessed using the gold standard reversible model parameters. Since there is no region in the human brain devoid of CB1R, tracer binding was quantified using the tracer plasma concentration. In addition to full kinetic modelling, we evaluated a simplified method of analysis based on tracer brain uptake for routine use of [^{18}F]MK-9470. Furthermore, we evaluated a simplified experimental approach that requires a few blood samples to obtain the required tracer plasma kinetics information and that may help eliminating the need for arterial sampling.

Materials and methods

Radiotracer characteristics and preparation

The precursor for the synthesis of [^{18}F]MK-9470 was obtained from Merck Research Laboratories and labelling was performed on-site using 2-[^{18}F]fluoroethylbromide [12]. The final product was obtained after high-performance liquid chromatography (HPLC) separation and had a radiochemical purity >95%. Specific activity was higher than 20 GBq/μmol. The tracer was administered in a sterile solution of 5 m*M* sodium acetate buffer with pH 5.5 containing 6% ethanol.

[^{18}F]MK-9470 metabolite analysis

Acetonitrile (1 ml) was added to 1 ml plasma and the mixture was centrifuged to precipitate protein. A 1-ml aliquot of the supernatant was filtered (Millex GV 0.22 μm, 13-mm diameter) and injected onto the HPLC system (Waters C18 XTerra, 5 μm, 4.6×250 mm, 1.5 ml/min, 50:50 acetonitrile/50 m*M* sodium acetate, pH 5.5). HPLC eluants from 0 to 5 min (fraction 1, metabolite fraction) and 5 to 10 min (fraction 2, parent fraction) were collected. The amount of radioactivity in each fraction was counted in a gamma counter to determine drug metabolism.

[^{18}F]MK-9470 free fraction measurement

The filter membrane of a Centricon Ultracel YM-10 centrifugal filter device was presaturated with 100 μl of a 10 μ*M* solution of MK9470. The solution was passed through the membrane by centrifugation for 30 min at 14 *g*. A 100-μl sample of plasma obtained 2 min after injection of [^{18}F]MK9470 was applied to the pretreated centrifugal filter device and passed through the membrane by centrifugation for 30 min at 14 *g*. Nonspecific binding to the membrane was assayed by adding protein-free plasma (PFP, obtained by centrifugal filtering using the same centrifugal device) spiked with 18.5 kBq [^{18}F]MK9470 that was passed through the filter by centrifugation for 30 min at 14 *g*. The assays were done each time in triplicate and the percentage free fraction was calculated as:

$$\text{free fraction } (\%) = 100 * \frac{\text{cps/g filtrate plasma 2 min post injection}}{\text{cps/g plasma} * \left(\frac{\text{cps filtrate PFP}}{\text{cps filter PFP} + \text{cps filtrate PFP}}\right)}$$

Subjects

All human imaging studies were conducted in the Division of Nuclear Medicine, University Hospital Leuven, Belgium. For kinetic modelling purposes, 12 healthy subjects (3 women, 9

men; 22–56 years old) were recruited in response to advertisements in local community newspapers and departmental websites. These 12 subjects participated in a test–retest study (panel 1) and a visual activation study (panel 2). Furthermore, 31 subjects from a previous age and gender study [15] were included for further validation of the simplified protocols (panel 3). All subjects were screened for neuropsychiatric and other medical disorders and underwent physical examination, blood and urine testing (including toxicology on the day of scanning, testing for all major known addictive drugs including Δ^9-THC). Exclusion criteria were as described previously [15]. The study was approved by the local ethics committee and performed in accordance with the World Medical Association Declaration of Helsinki. Written informed consent was obtained from all the volunteers prior to the study.

Imaging procedure

Images were acquired using a HR+PET camera (Siemens, Erlangen, Germany) (panels 1 and 3) or a HiRez Biograph16 PET/CT camera (Knoxville, TN) (panel 2), depending upon their availability at the time the studies were conducted. Studies in the same subject were conducted using the same camera. HR+PET data were acquired in three-dimensional mode and were reconstructed using a three-dimensional reprojection algorithm including scatter and measured attenuation correction (^{68}Ge source). For the studies conducted on the HiRez Biograph16 PET/CT camera, a low dose (80 kV tube potential, 11 mAs) CT scan without contrast agent was performed at the beginning of each PET segment for attenuation correction. Images were reconstructed using a three-dimensional OSEM (ordered-subset expectation-maximization) iterative reconstruction with five iterations and eight subsets and post-smoothing with 3-D gaussian (FWHM 6 mm) [16]. Standard PET image procedures were followed in all subjects as described by Van Laere et al. [15] and Burns et al. [13]. MR images were obtained for anatomical coregistration with the PET images [15].

Panel 1: Long duration and test–retest studies

Two healthy subjects (one woman, 24 years old, and one man, 23 years old) were scanned for 700 min following tracer injection using the HiRez Biograph16 camera. The scanning protocol consisted of seven scanning segments. The first segment started upon injection (approximately 370 MBq) and consisted of 22 frames with a progressive increase in frame duration (4×15, 4×60, 5×180, 4×300 and 5×600 s) and a total duration of 90 min. The following three segments had a total duration of 60 min each (6×10-min frames) starting at approximately 120, 210 and 300 min. The last three segments had a total duration of 40 min starting at approximately 420 min (2×20-min frames), 540 min (2×20-min frames) and 660 min (a single 40-min frame). The free fraction of [^{18}F]MK-9470 in plasma was measured in these two subjects.

Short-term test–retest reproducibility was evaluated in four healthy male subjects (age 24±1 years). Each subject was scanned twice using the HR+PET camera with approximately 24 h between scans. For the first two subjects, the scanning protocol had a total duration of 360 min and consisted of the first four scanning segments as described above. For the last two subjects in the test–retest studies, the scanning protocol had a total duration of 180 min and consisted of the first two segments only. Arterial blood sampling for measuring total activity and tracer metabolism in plasma was performed manually in all subjects as described by Burns et al. [13]. For the last two subjects, venous samples were also taken during the two scans to measure tracer metabolism and total activity at 10, 20, 40, 60, 90, 120 and 180 min after tracer injection.

Panel 2: Visual activation study

The potential effect of blood flow on [^{18}F]MK-9470 brain kinetics was investigated in a group of six healthy subjects (two women, four men, 35±14 years of age). Subjects were studied under control and visual activation in a balanced design (baseline–stimulation and stimulation—baseline, three subjects each). Studies took place on separate days, 4–10 days apart. In the control condition, the scanner environment was darkened and quiet and subjects were scanned with their eyes covered. During the activation condition subjects watched and listened to a popular action movie (*Déjà Vu*; Touchstone Pictures, USA) on an 8-inch LCD screen placed in front of them but just outside the field of view. Except for the first subject, the scanner tunnel was back-lit with an 80-W lamp. Each [^{18}F]MK-9470 study was preceded by two perfusion studies with $H_2{}^{15}O$ for measurement of cerebral blood flow (CBF). The subjects received the first baseline $H_2{}^{15}O$ scan about 15 min before the condition started with their eyes open and ears unplugged in a quiet, dimly-lit environment. The second $H_2{}^{15}O$ scan was acquired 3 min after the start of the condition, followed by the [^{18}F]MK-9470 scan 15 min after the condition started.

For the perfusion studies, a bolus of approximately 300 MBq of $H_2{}^{15}O$ was injected over 30 s using a syringe pump. Data acquisition was started immediately after injection. Data were acquired in list mode and reconstructed in 6×30-s frames. Only the first two frames were taken for subsequent data analysis [17, 18]. The [^{18}F]MK-9470 PET scan consisted of two scanning segments separated by a 15-min break. The first segment started with tracer injection (190±20 MBq) and consisted of 26 frames with

a progressive increase in frame duration (4×15, 4×60, 2×150 and 16×300 s) and a total duration of 90 min. The second segment consisted of nine 300-s frames for a total duration of 45 min. Arterial sampling was performed in all subjects following the procedure in panel 1 and the free fraction of [^{18}F]MK-9470 in plasma was measured in five subjects in this panel. [^{18}F]MK-9470 and perfusion scans were conducted using the HiRez Biograph16 camera.

Panel 3: Extended healthy volunteer group

Data from the 31 subjects of the age and gender study who had undergone full arterial sampling as described in Van Laere et al. [15] were also included in this work. Data were acquired using the HR+PET camera and consisted of a 75-min and a 30-min segment separated by a 15-min break. Blood sampling was performed as in panel 1.

Image analysis

The MR volumetric image, and [^{18}F]MK-9470 (first segment) and $H_2{}^{15}O$ summed PET images were coregistered using SPM99 (http://www.fil.ion.ucl.ac.uk/spm). The additional PET segments were aligned with the first PET segment using in-house developed analysis software written in Matlab (Mathworks, Tulsa, OK; version 6.5, release 13). Then, using the MRI scan for anatomical delineation, irregular regions of interest (ROIs) were drawn for each subject (bilaterally) in the caudate, putamen, thalamus, midbrain, anterior and posterior cingulate gyrus, frontal, parietal, occipital, medial and lateral temporal cortices, cerebellum, pons and white matter (centrum semiovale) using the Montreal Neurological Institute's DISPLAY software (http://noodles.bic.mni.mcgill.ca/ServicesSoftware/HomePage). Special attention was given to the ROIs in the occipital region in panel 2 subjects where the primary and associative visual cortices were considered separately. Since the spatial resolution of PET and MRI images does not allow the exact border between the striate cortex and the visual areas surrounding it to be distinguished, the primary visual cortex included Brodmann area 17 and part of area 18. [^{18}F]MK-9470 tissue time–activity curves (TAC) were expressed in SUV (standardized uptake value) using each subject's weight and the corresponding tracer injected dose: TAC (SUV)=TAC (Bq/cm^3) × 1,000 cm^3/kg × subject's weight (kg)/injected dose (Bq). TAC creation and all subsequent analyses were performed using in-house developed analysis software written in MATLAB.

Kinetic modelling

The [^{18}F]MK-9470 tracer input function was obtained by multiplying the measured total activity and the metabolite fraction $f(t)$ obtained by fitting the measured plasma metabolite fraction to the Hill function given by:

$$f(t) = 1 - at^n/(t^n + b) \quad (1)$$

The parameters a, b and n were estimated for each study. Exponential functions were also considered. When using a monoexponential function the parent fraction after 160–180 min following tracer injection was overestimated and the half-time of a second exponential could not be identified in most cases.

CB1R availability was estimated using standard compartmental modelling with the metabolite-corrected arterial input function. Three different reversible compartmental models were considered: (1) a single-tissue model with rate constants K_1 and k_2, $V_T=K_1/k_2$ [19]; (2) a two-tissue model with rate constants K_1 and k_2 ($V_{ND}=K_1/k_2$) and the tracer binding rate to and off the receptors, k_3 and k_4, respectively; and (3) a two-tissue model with a k_4 constant throughout the brain. When using configuration 3, k_4 was estimated by simultaneously fitting several brain regions displaying high, intermediate and low tracer uptake and then K_1, k_2 and k_3 were estimated for individual regions.

An irreversible model with two tissue compartments described by the rate constants K_1 and k_2 and the tracer binding rate to the receptors, k_3 ($k_4=0$) was also considered. The vascular contribution (V_B) to the tissue TACs was included as an additional parameter in all compartmental models.

Parameters were estimated by fitting the tissue TACs to the reversible or irreversible compartment model and the parameter coefficients of variation were obtained from the covariance matrix resulting from the model sensitivity function [20, 21] and expressed as percentage of the parameter value (%COV). The data were fitted using the *lsqcurvefit* MATLAB function using Simulink to compute the convolution integrals.

When using the data-driven approach, the system impulse response function was estimated using spectral analysis [22, 23] and non-negative least squares (using the *lsqnonneg* MATLAB function). The tissue response is obtained from the convolution of the system impulse response function with the tracer plasma concentration, $C_P(t)$:

$$TAC(t) = \sum_{i=1}^{n} \alpha_i e^{-\beta_i t} \otimes C_P(t) + V_B C_B(t) \quad (2)$$

A set of $n=100$ logarithmically distributed β_i values were selected in the interval $[\beta_{min}, \beta_{max}]$. Fits were performed on non-decay-corrected PET data. Therefore the slowest possible component β_{min} was set using the half-life of ^{18}F: $\beta_{min}=\lambda$, with $\lambda=\ln(2)/110$ min. The upper limit was set to $\beta_{max}=6$ min^{-1}. The total activity in plasma was used instead of the total activity in blood, C_B, to take

account of the vascular contribution to the measured tissue activity. For both reversible and irreversible systems, the tracer delivery to the tissue or rate constant K_1 is given by $\sum_{i=1}^{n} \alpha_i$. For a reversible system, the tracer V_T is given by $\sum_{i=1}^{n} \alpha_i/\beta_i$ and β_{min} slightly larger than $\lambda(\beta_{min}=1.05\lambda)$ to avoid estimation of infinite V_T values. For irreversible tracer binding $\beta_{i\neq n}>\lambda$ and $\beta_n=\lambda$, and the net irreversible uptake rate constant K_i is equal to α_n. Although the K_i obtained from the data-driven method is equivalent to the value estimated using Patlak analysis [22], no assumption about the time to reach equilibrium was made when fitting the data to Eq. 2. Furthermore, information about tracer delivery to the brain or K_1 and V_B can be obtained when fitting the data.

Besides the kinetic modelling methods, a nonmodelling approach based on the shape of the brain tissue curves and the integral of the tracer plasma concentration was used to estimate [^{18}F]MK-9470 specific binding [24, 25]. The [^{18}F]MK-9470 fractional uptake rate (FUR) was calculated as the ratio of tracer concentration in tissue at the end of the scan, TAC_T, to the integral of plasma activity from the time of injection to the end of the scan:

$$FUR = TAC_T \Big/ \int_0^T C_p(t)dt \qquad (3)$$

The stability of reversible and irreversible tracer binding parameters with respect to scan time was evaluated by analysing the PET data with subsequent reductions in interval, i.e. from 0 to 700 min, 0 to 360 min and 0 to 180 min (depending on the total scan time data available). Furthermore, the ability of K_i and FUR to quantify CB1R availability was assessed by comparing these parameters to the gold standard parameters from reversible tracer kinetic analysis V_T and $V_{ND}k_3$ which is proportional to CB1R availability and equivalent to k_4BP_p (BP_p denotes the tracer binding potential not corrected for plasma protein binding in plasma) [19]. The parameter $V_{ND}k_3$ is not a function of blood flow and provides receptor availability information [26].

The effects of blood flow on [^{18}F]MK-9470 brain uptake, on estimation of binding parameters and on the rate constant K_1 were assessed in six subjects (panel 2). K_1 values were determined using the first 15 min following [^{18}F]MK-9470 injection [26] by means of spectral analysis. [^{18}F]MK-9470 binding parameters and K_1 values were compared to the regional CBF values determined from the perfusion studies performed immediately before [^{18}F]MK-9470 tracer injection. Since no arterial sampling was performed during the $H_2{}^{15}O$ PET scans, only relative CBF values were calculated using the radioactivity in the first two frames. Regional values were divided by the total brain uptake to obtain normalized CBF (nCBF).

Simplification of [^{18}F]MK-9470 scanning protocol

We explored the possibility of simplifying the [^{18}F]MK-9470 scanning protocol and analysis of human studies by avoiding arterial sampling and using a limited number of venous samples for measuring plasma activity and tracer metabolism. Additionally, we evaluated the use of the tracer concentration in tissue at the end of the scan TAC_T expressed in SUV (see Eq. 3) as an index of tracer binding as used in previous studies with this tracer [13, 15] and recently also evaluated for [^{11}C]MePPEP [27].

Results

Plasma kinetics

[^{18}F]MK-9470 percentage fractions in arterial samples are shown in Fig. 1 for subjects in panels 1 and 2. At 10 min, 79±9% (n=22) of the total radioactivity in arterial plasma corresponded to [^{18}F]MK-9470. This fraction declined to 35±8% (n=22) at 60 min, 19±6% at 120 min, and 13±5% at 180 min. The intact fraction of [^{18}F]MK-9470 was about 5% from 270 min (n=6) to 600 min (n=2). For all scans, the [^{18}F]MK-9470 input curves obtained after metabolite correction decreased with time (Fig. 1). The plasma protein binding of [^{18}F]MK-9470 was assessed in five of the six subjects in panel 2 and measurements were performed during both control and visual activation studies in three of the subjects (Table 1). The average [^{18}F]MK-9470 plasma protein binding was 95.5±1.4% (n=8).

Brain kinetics

[^{18}F]MK-9470 exhibits slow brain kinetics reaching a plateau between 90 and 120 min after bolus injection. Tracer uptake remains relatively constant up to 460 min while plasma tracer concentration still decreases up to 480 min (Fig. 1). In the two subjects scanned for 700 min, the uptake between 300 and 360 min was on average 10% and 12% higher in gray matter regions (pons not included) than the uptake between 540 and 580 min and between 660 and 700 min, respectively. In the pons, equivalent percentages were 15% and 25%. The noise content in images acquired at these late times was considerable (Fig. 2).

Modelling

Reversible models

The reversible single-tissue compartment model was not sufficient to describe [^{18}F]MK-9470 brain kinetics, with a general overestimation of tracer uptake between 120 and

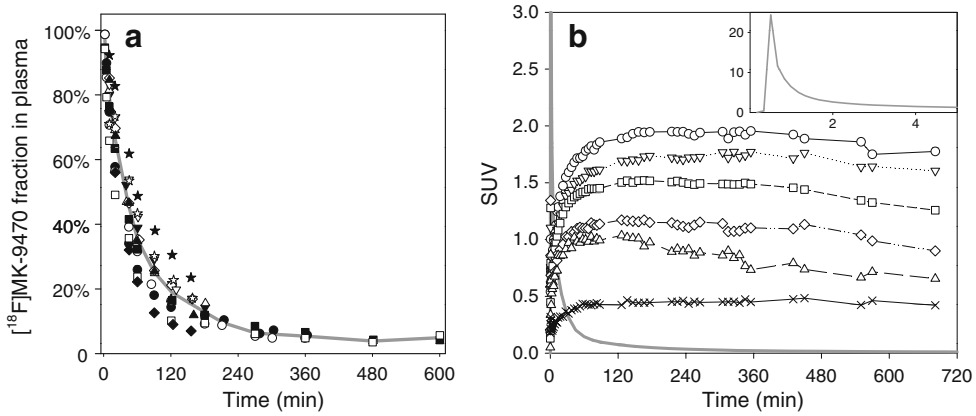

Fig. 1 [^{18}F]MK-9470 plasma and brain kinetics. **a** Average [^{18}F]MK-9470 percentage fraction in arterial samples measured in the 12 subjects participating panels 1 and 2 of the study (*solid line*). *Symbols* represent the individual subject fractions (average of two measurements for each of ten subjects). **b** Regional [^{18}F]MK-9470 kinetics in the human brain: ○ putamen, ∇ cingulate gyrus, □ occipital cortex, ◊ thalamus, Δ pons and × white-matter; *solid line* shows the arterial plasma input function (*insert* tracer input function during the first 5 min after tracer injection). The data are corrected for physical decay of ^{18}F

270 min, and underestimation at early time points (t<60 min) and at later time points (t>270 min) in the studied regions (Fig. 3). Furthermore, V_T estimates were highly dependent on scan length (Fig. 4), indicating that stable estimation of V_T is not possible using a single-tissue compartment model. V_T values estimated using data up to 700 min (two subjects) were on average 22% higher than values estimated using 360-min data (linear regression slope 1.22, r^2=0.93). V_T values estimated using data up to 270, 180 and 90 min were underestimated relative to the 360-min values by 13% (slope 0.87, r^2=0.98), 31% (slope 0.69, r^2=0.98) and 58% (slope 0.42, r^2=0.98), respectively. K_1 estimates were stable when considering different scan lengths. In the gray matter K_1 values were within 0.010 and 0.045 with %COV<3% in all regions.

Using the reversible data-driven method, two main peaks were observed within the spectrum in all regions. One of the peaks was observed around β_{min}, consistent with the slow tracer kinetics. The second peak, observed around $\beta = 10^{-3}$, could be associated with a faster component probably reflecting the nondisplaceable compartment. The contribution of this faster component to the measured TAC was less than 20% at 180 min. As with the single-tissue model, V_T estimates using the data-driven method were dependent on scan length.

Table 1 [^{18}F]MK-9470 plasma protein binding (panel 2 subjects)

Subject no.	Visual activation	Control
1	n/a	n/a
2	95.25%	n/a
3	n/a	95.37%
4	95.02%	92.40%
5	96.65%	96.52%
6	96.15%	96.31%

No further analyses were performed with the single-tissue model or the reversible data-driven methods.

Fits improved after a second tissue compartment was introduced (Fig. 3). However, rate constants k_2, k_3 and k_4 could not be identified for individual regions. Parameter estimates were highly dependent on initial conditions and %COV values were higher than 50% in most cases. Therefore, the off-binding rate k_4 of [^{18}F]MK-9470 from CB1R was assumed to be constant throughout the brain and TACs from regions with high, intermediate and low activity uptake were fitted simultaneously to a two-tissue compartment model for estimating the brain k_4. A unique solution for k_4 was possible in all cases (%COV<10%) for both the 700 and 360-min data (four subjects, six scans, panel 1), but it was not possible to reliably estimate k_4 using PET data up to 180 min. In the two subjects scanned for 700 min, k_4 was 0.0033 min^{-1} using data up to 700 min and 0.0036 min^{-1} using up to 360 min. The average k_4 value for the six 360-min scans was 0.0041±0.0010 min^{-1}. The k_4 values were on average ten times smaller than the K_1 values.

Parameters K_1, V_{ND} and k_3 were estimated for individual regions by fixing k_4 to the value estimated from the simultaneous fitting step. Parameters K_1 and V_B could be identified, but the k_2 and k_3 estimates were dependent on initial conditions with %COV as large as 40%. An inverse correlation between $V_{ND}=K_1/k_2$ or the distribution volume of the nonspecific and free tracer in the brain and k_3 was observed, resulting in a stable estimate for the total volume of distribution $V_{T\text{-}2C}=V_{ND}(1+k_3/k_4)$ and for $V_{ND}k_3$. The F-statistics showed that a two-tissue model with global k_4 produced a statistically better fit (p<0.001) than a single-tissue model. The stability of $V_{T\text{-}2C}$ and $V_{ND}k_3$ estimates with respect to scan length is shown in Fig. 4. The good agreement between the parameters estimated using 700 min, 360 min and 180 min (with k_4=0.0041 min^{-1}

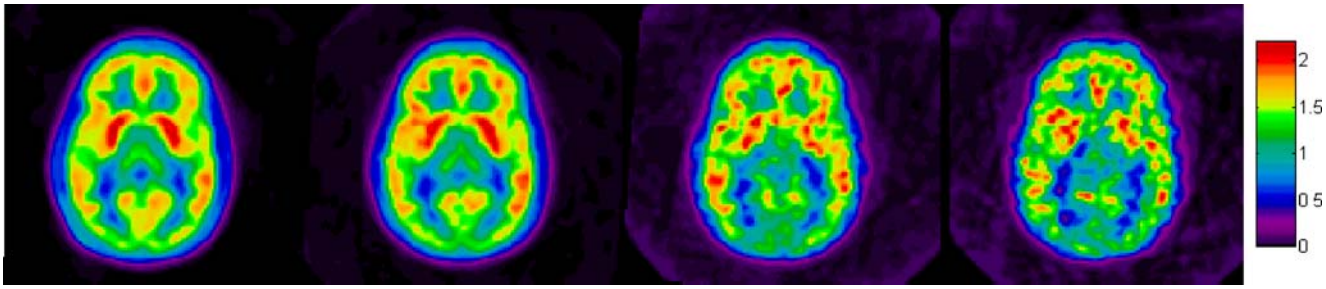

Fig. 2 Uptake of [^{18}F]MK-9470 in human brain: *left to right* average uptake during the periods 120–180 min, 300–360 min, 540–580 min and 660–700 min, respectively, after administration of a tracer bolus of approximately 370 MBq. Data are expressed in SUV and corrected for physical decay of ^{18}F

estimated using the 360-min scan length) suggests that a 180-min scan is sufficient to estimate CB1R availability when using a population-based k_4 value. The test–retest variability estimated as 1 − parameter (day 2)/parameter (day 1) was between 10% and 30% for both $V_{T\text{-}2C}$ and $V_{ND}k_3$ in regions with high and low tracer binding when using a scan length of 180 or 360 min. The relationship between $V_{ND}k_3$ estimated on day 1 and day 2 (four subjects in panel 1) using the 360-min scan length is shown in Fig. 6, and average regional values and test–retest variability values for $V_{T\text{-}2C}$ and $V_{ND}k_3$ are shown in Tables 2 and 3, respectively.

Irreversible models

The small k_4 value and the slow tracer clearance from tissue throughout the brain suggest that [^{18}F]MK-9470 clearance from the receptor can be considered negligible for the duration of the scan and therefore data can be described using irreversible tracer kinetics for estimating receptor availability.

When using the irreversible compartmental model, multiple solutions with similar cost function values were found for k_2 and k_3 and no clear correlation was observed between the two parameters, as has been shown previously for other tracers [28], or between V_{ND} and k_3 as with the reversible two-tissue compartment model. In contrast, the fit of the kinetic data to Eq. 2 was satisfactory in all regions considered using the data-driven approach with a trap in the system ($\beta_{i\neq n}>\lambda$ and $\beta_n=\lambda$). Furthermore, the stability of K_i estimates with respect to scan length was excellent (Fig. 5). Very good agreement between K_i values estimated for scan lengths of 700 and 360 min (slope 0.98, intercept set to zero; $r^2>0.99$) and between K_i values estimated for scan lengths of 360 and 180 min (slope 1.04, intercept set to zero; $r^2>0.99$). The possibility of further shortening the scanning time was assessed by comparing the K_i values estimated using 120–130 min (the first point in the second segment in the panel 1 dataset) against the values obtained using 180 min. Good agreement was found between both sets of K_i values (Fig. 5) with the slope of the linear regression being between 0.88 and 1.05 ($r^2>0.99$). Test–retest variability estimated as 1 − K_i (day 2)/K_i (day 1) was in the range ±10% for the four subjects when using the 180-min scan length (Fig. 6, Table 3). The test–retest variability increased when using the 120-min data, especially for one of the subjects (3% versus 17%).

Figure 3 shows typical fits of tissue curves using the irreversible data-driven method and the reversible two-tissue model. Both approaches resulted in similar fits and cost function values, but the reversible model slightly overestimated tracer uptake between 30 and 60 min in cortical regions, the striatum and the cerebellum. As shown in Fig. 7, a fairly linear relationship between $V_{T\text{-}2C}$ and K_i and $V_{ND}k_3$ and K_i was observed. When the intercept of the linear regressions was included as a parameter in the linear fits, the resulting slope values changed by less than 5% and the respective intercept values were negligible. These results suggest that K_i provides information on [^{18}F]MK-

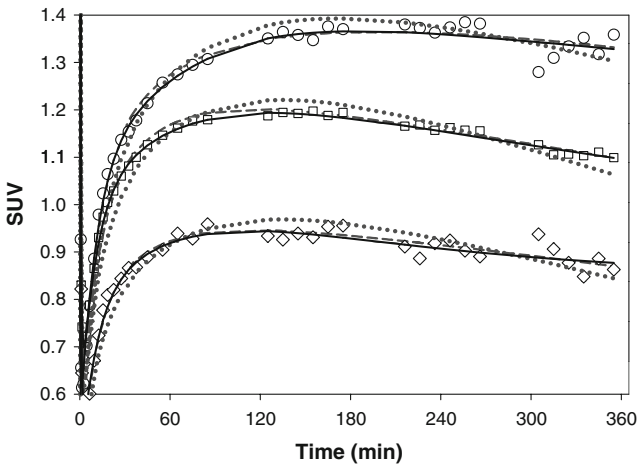

Fig. 3 Typical fits of [^{18}F]MK-9470 TACs using a one-tissue reversible model (*dotted lines*), a two-tissue reversible model (*dashed lines*) and data-driven methods (*solid lines*) (○ putamen, □ occipital cortex, ◊ thalamus). The F-statistics showed that the data were statistically better described using the two-tissue model with global k_4 than using the single-tissue model ($p<0.001$)

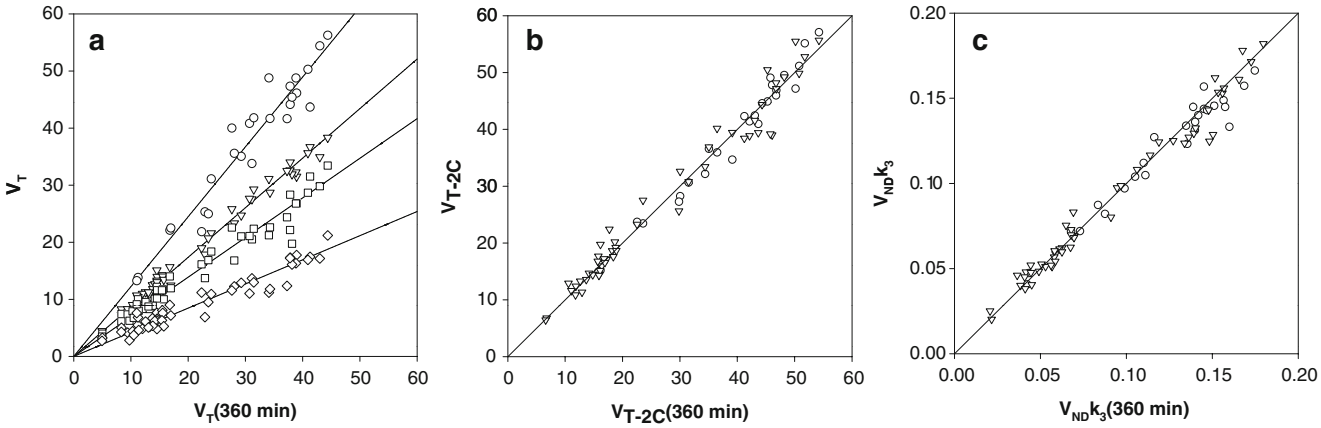

Fig. 4 Effects of scan length on estimation of reversible model parameters. **a** Single-tissue model (four subjects; average value for the two subjects receiving two scans): ○ V_T 700 min vs. V_T 360 min, ∇ V_T 270 min vs. V_T 360 min, □ V_T 180 min vs. V_T 360 min, ◊ V_T 90 min vs. V_T 360 min; *solid lines* linear regressions (r^2>0.91) between variables (intercept set to zero). **b** Two-tissue compartment model (four subjects; average parameter values for the two subjects receiving two scans): ○ $V_{T\text{-}2C}$ 700 min vs. $V_{T\text{-}2C}$ 360 min (slope=1.0, r^2>0.97), ∇ $V_{T\text{-}2C}$ 360 min vs. $V_{T\text{-}2C}$ 180 min (slope=0.99, r^2>0.97). **c** ○ $V_{ND}k_3$ 700 min vs. $V_{ND}k_3$ 360 min (slope=0.97, r^2>0.95, *solid line)*, ∇ $V_{ND}k_3$ 180 min vs. $V_{ND}k_3$ 360 min (slope=0.98, r^2>0.98, *dashed line*)

9470 binding to CB1R and that the nonspecific binding of the tracer is very small.

Simplified models

In addition to applying tracer kinetic modelling to estimate net irreversible uptake rate constant K_i, a simplified approach based on the shape of the brain tissue curves [24] was used to calculate the FUR of [^{18}F]MK-9470 (Eq. 3). Due to the slow [^{18}F]MK-9470 brain kinetics, it was possible to obtain a very reliable value for the tissue uptake at a given time T or TAC_T from the average of the PET frames acquired around the time of interest. In panels 1 and 2, both K_i and FUR values were calculated using data between 120 and 180 min. Additionally, data between 90 and 120 min were used for all panels. As shown in Fig. 8, [^{18}F]MK-9470 FUR values were highly correlated with K_i estimates using kinetic analysis. When using data up to 180 min, the individual slopes for the linear regression (K_i vs. FUR) were between 0.91 and 1.04 (r^2>0.99, 22 scans in panels 1 and 2). When using 120-min scan length data, the individual slopes for the linear regression were between

Table 2 Average volumes of distribution of [^{18}F]MK-9470 ($V_{T2\text{-}C}$ and $V_{ND}k_3$), FUR and area under the tissue curves (AUC) for the subjects participating the study. Values are means±SD

ROI	Panels 1 and 2 (12 subjects)				Panel 3 (31 subjects)		
	$V_{T\text{-}2C}$	$V_{ND}k_3$ (min^{-1})	FUR (min^{-1} ×10^3)	AUC (SUV)	K_i (min^{-1} ×10^3)	FUR (min^{-1} ×10^3)	AUC (SUV)
Caudate	23.4±12.0	0.079±0.04	17.1±8.8	1.38±0.22	17.3±5.6	17.9±5.5	1.43±0.24
Putamen	25.1±13.3	0.085±0.04	19.6±9.6	1.59±0.27	19.1±6.2	19.8±5.5	1.58±0.24
Thalamus	12.6±7.6	0.045±0.02	12.9±5.8	1.06±0.16	12.5±4.3	13.4±4.5	1.07±0.18
Midbrain	14.1±8.8	0.050±0.02	12.3±5.7	1.01±0.13	11.5±3.7	12.1±3.8	0.97±0.14
Anterior cingulate gyrus	24.5±13.9	0.082±0.04	17.6±8.7	1.43±0.21	16.3±5.8	16.9±5.7	1.34±0.19
Posterior cingulate gyrus	23.1±13.9	0.078±0.04	18.4±9.3	1.49±0.23	17.9±6.0	18.6±6.1	1.48±0.21
Frontal cortex	22.4±13.1	0.076±0.04	17.0±8.3	1.39±0.23	16.0±5.4	16.8±5.6	1.34±0.20
Parietal cortex	21.6±13.4	0.073±0.04	16.7±8.3	1.36±0.22	15.9±5.4	16.6±5.5	1.32±0.22
Temporal cortex	21.3±12.8	0.078±0.04	17.2±8.5	1.40±0.22	15.4±5.2	16.2±5.4	1.29±0.21
Occipital cortex	17.7±11.3	0.073±0.04	16.4±7.9	1.33±0.19	14.8±5.2	16.1±5.5	1.28±0.20
Cerebellum	15.8±10.5	0.061±0.03	15.5±7.6	1.26±0.20	13.2±4.5	14.2±4.6	1.13±0.16
Pons	7.7±5.7	0.056±0.03	10.4±5.2	0.84±0.12	9.9±4.1	11.1±4.2	0.87±0.12
White matter	5.4±4.4	0.028±0.01	5.0±2.3	0.41±0.06	4.8±1.6	5.1±1.6	0.40±0.06

Table 3 Test–retest variability of [^{18}F]MK-9470 binding parameters for subjects in panel 1 calculated as the average of the absolute value of 100% [1 − parameter (day 2)/ parameter (day 1)]. Values are mean±SD (n=4)

ROI	$V_{T\text{-}2C}$	$V_{ND}k_3$ (min^{-1})	FUR (min^{-1} ×10^3)	AUC (SUV)
Caudate	21±9%	16±6%	3±3%	3±3%
Putamen	17±9%	9±13%	3±3%	4±3%
Thalamus	35±24%	11±8%	3±1%	3±2%
Midbrain	37±50%	12±9%	3±2%	5±2%
Anterior cingulate gyrus	16±13%	13±11%	5±4%	6±3%
Posterior cingulate gyrus	16±12%	11±8%	1±1%	4±4%
Frontal cortex	22±17%	8±11%	4±3%	5±2%
Parietal cortex	26±9%	9±5%	1±1%	4±4%
Temporal cortex	15±14%	12±10%	4±3%	5±2%
Occipital cortex	30±20%	10±10%	3±1%	4±2%
Cerebellum	23±9%	8±9%	3±2%	4±2%
Pons	16±10%	5±3%	5±4%	6±4%
White matter	36±29%	20±18%	5±4%	5±5%

0.87 and 1.03 (r^2>0.99, 53 scans). As with K_i, FUR test–retest variability was below 10% when using data between 120 and 180 min to estimate TAC_T (Table 3). The variability increased slightly when TAC_T was estimated using the PET data in the 90–120 min interval.

The between-subject variability for both FUR and $V_{ND}k_3$ was large, up to 55% (SD/average) for subjects in panels 1 and 2. For example, the $V_{ND}k_3$ and FUR values in the putamen were in the ranges 0.18–0.038 and 0.010–0.040 min^{-1}, respectively. In the thalamus equivalent values were in the ranges 0.083–0.021 and 0.007–0.024 min^{-1}, respectively. The subjects in panel 3 had a wider age spread. The between-subject variability in this group was around 35%. Regional values are given in Table 2.

Blood flow independence

One of the main concerns with slow or irreversible tracer kinetics is that the parameter used to characterize the tracer-specific binding could be mostly determined by blood flow through K_1 and not k_3. The highest increase in nCBF during the video watching task relative to the control condition was observed in the primary visual areas (Brodmann areas 17 and 18), whereas a modest increase was observed in Brodmann area 19. Table 4 shows nCBF values in primary visual areas together with the K_1, K_i and FUR values for the [^{18}F]MK-9470 dynamic study following the perfusion scan. K_1 values were relatively small throughout the brain (mostly <0.05 ml/cm^3/min, gray matter average 0.028±

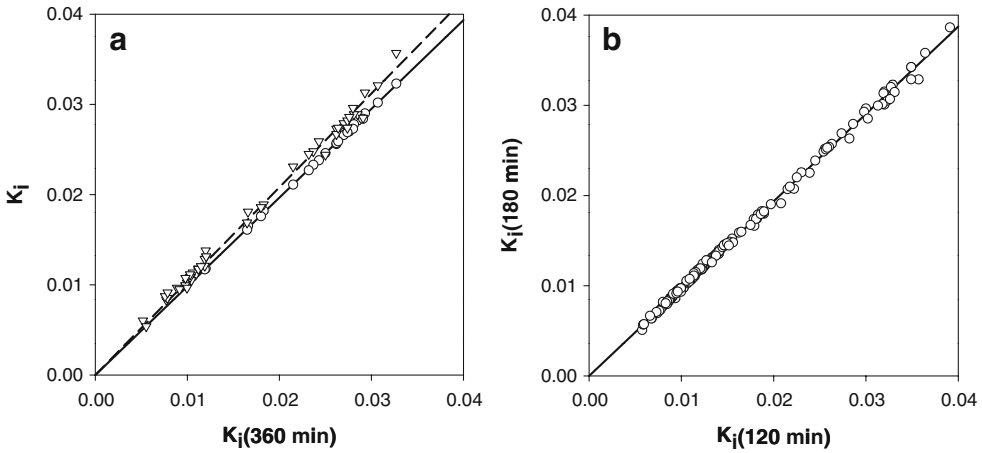

Fig. 5 Effects of scan length on estimation of irreversible model parameters. **a** K_i (data-driven method, four subjects; average values for the two subjects receiving two scans): ○ K_i 700 min vs. K_i 360 min (slope=0.98, r^2>0.99, *solid line*), ∇ K_i 180 min vs. K_i 360 min (slope=1.04, r^2>0.99, *dashed line*). **b** K_i (data-driven method, average parameters for the subjects receiving two scans in panels 1 and 2): Correlation between K_i estimated using 180-min and 120-min data (*solid line* linear regressions between variables with intercept set to zero; slope=0.97, r^2>0.97)

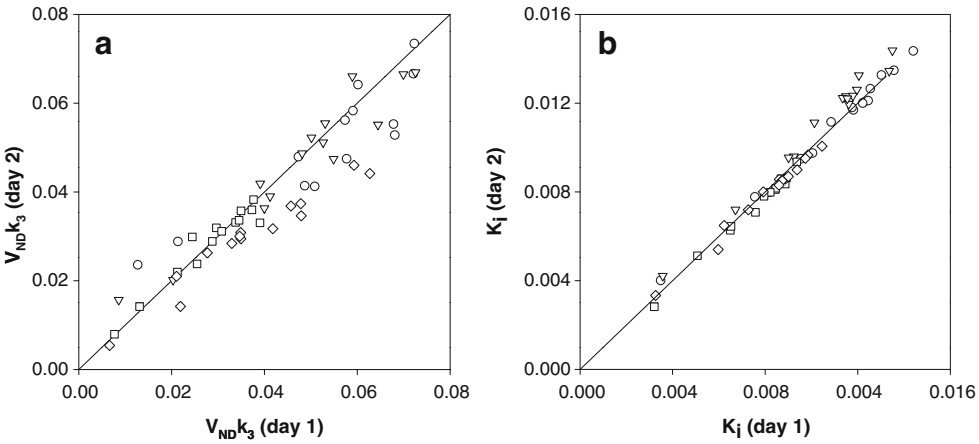

Fig. 6 Test–retest variability of $V_{ND}k_3$ (**a**) and K_i (**b**); parameters estimated using a scan length of 360 min. *Symbols* show the data for the four subjects in panel 1 scanned on two occasions for at least 180 min; the *solid line* represents the line of identity

0.013 ml/cm^3/min, 264 regions) in all subjects and there was no correlation between K_i or FUR and K_1. Furthermore, the K_i and FUR values in the primary visual cortex were almost identical in both conditions whereas a significant change in nCBF was observed during the watching video condition. For all subjects, the K_i and FUR values during the visual activation and control tasks were within ±10% of each other in all regions, calculating changes as 1 − parameter (visual activation)/parameter (control). Similar results were obtained when using 120-min data to calculate K_i and FUR for five of the six subjects. In the sixth subject, a global increase in TAC_T (120 min) of about 20% was observed during the activation relative to the blind condition, whereas only a small increase was observed in FUR values (6%).

Simplification of [^{18}F]MK-9470 scanning protocol

The excellent correlation between K_i and FUR values supports the use of a 30- or 60-min PET scan about 1.5 to 2 h after tracer administration for accurately estimating tracer activity. Therefore, the possibility of simplifying the blood sampling scheme was investigated by initially using a shorter input curve. There was an excellent correlation between the integral of the tracer arterial input function from injection time to 60 min and to 180 min (r^2=0.98, n=22) with the integral from 0 to 60 min being on average 20% lower than the integral from 0 to 180 min. When using a 60-min input curve, the FUR test–retest variability and the FUR change during the visual activation study were within 10% in all regions.

Figure 9a compares the [^{18}F]MK-9470 plasma concentration measured in arterial and venous samples in two subjects from the test–retest panel. The curves in both subjects were very similar suggesting that from 10 min after injection, the tracer input curve could be estimated using venous samples. The relationship between the integral of the tracer arterial input function from the time of injection to 180 min and the AUC of [^{18}F]MK-9470 plasma concentration measured using only four samples at 10, 20, 45 and 60 min is also shown in Fig. 9b. Both quantities showed a good correlation (r^2=0.88, n=22) and the integral of the plasma curve was on average 2.7 times smaller using these four data points than when using the whole curve up to 180 min (about 31 samples). The relationship between FUR values estimated using both curves is shown in Fig. 9c. The bias introduced by using only four samples

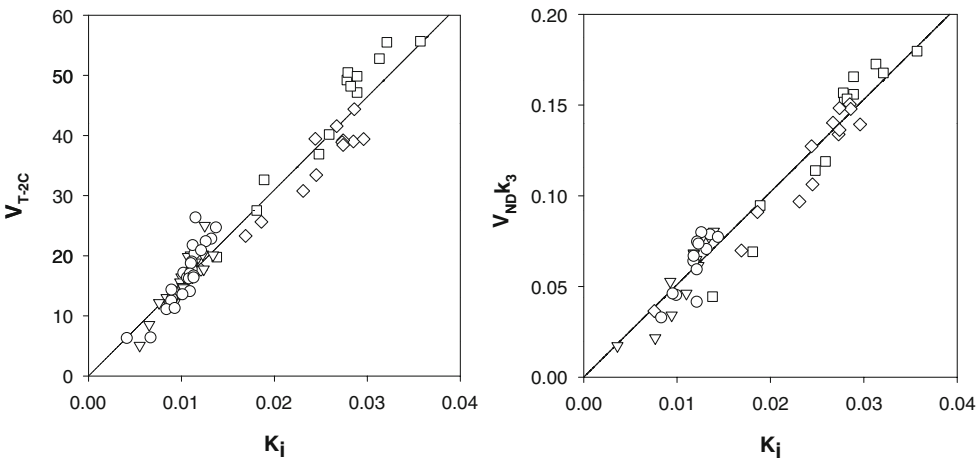

Fig. 7 Correlation between [^{18}F]MK-9470 net irreversible uptake rate constant K_i and the two-tissue compartmental model parameters $V_{T\text{-}2C}$ and $V_{ND}k_3$. *Symbols* show the parameters for subjects scanned for at least 360 min (average of 2 scans for 2 subjects); the *solid line* shows the linear regression between the two parameters ($V_{T\text{-}2C}$=1548 K_i, r^2=0.96 and V_{ND} k_3=5.1 K_i, r^2=0.94)

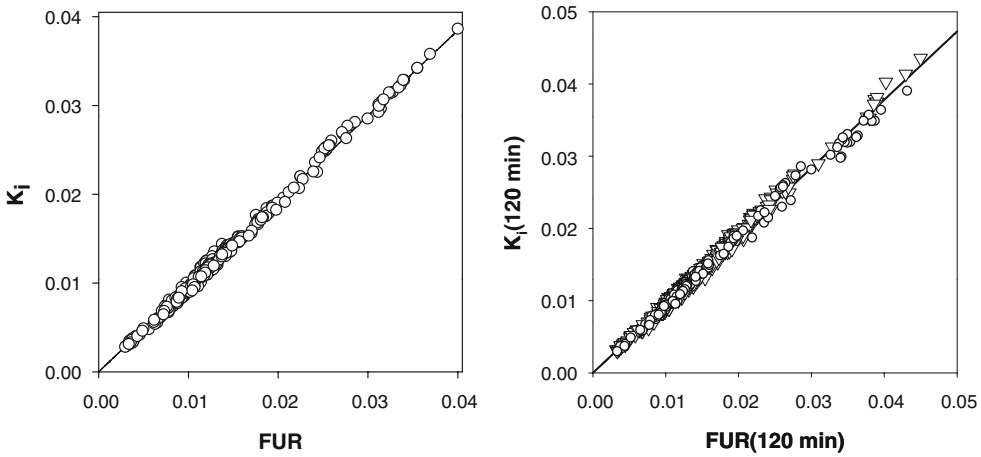

Fig. 8 The relationship between [^{18}F]MK-9470 K_i values from kinetic analysis and FUR. **a** Parameters estimated using data up to 180 min from subjects in panels 1 and 2. The *solid line* shows the linear regression between the two parameters; average of two measurements for subjects receiving two scans) (K_i=0.96 FUR; r^2> 0.99). **b** Parameters estimated using data up to 120 min for all subjects (○ panels 1 and 2, ∇ panel 3. The *solid line* shows the linear regression between the two parameters; average of two measurements for subjects receiving two scans) (K_i=0.95 FUR; r^2=0.99)

was consistent for all subjects with the individual linear regression slopes in the interval 0.31–0.44. Besides, the test–retest variability and the change during the visual activation task relative to the control task of the FUR value estimated with the four samples were below 10% in all subjects. These results suggest that the use of a few venous samples together with a short scan starting about 120 min after injection may be an adequate alternative for [^{18}F]MK-9470-specific binding estimation.

Figure 10 shows the relationship between [^{18}F]MK-9470 FUR values and the TAC_T for all subjects in the study. The slope of the linear regression between TAC_T and FUR was highly variable between subjects (between 0.007 and 0.030 min^{-1}), mostly due to the variability of the plasma input integral.

The test–retest variability of TAC_T was excellent (<7%) and, except for one subject in panel 2, the changes in TAC_T between conditions were similar to the test–retest variability. The last subject in this panel showed a global TAC_T increase of about 20% during the activation condition relative to the blind condition. No significant difference in FUR values was observed in this subject. Between-subject variability was markedly lower using TAC_T values (15%) than using K_i and FUR estimates (Table 2), similar to values previously reported [15] and similar to findings using [^{11}C]MePPeP [27].

Discussion

In this work we evaluated reversible and irreversible tracer kinetic modelling approaches as well as a simplified analysis method based on the tracer uptake in the brain for analysing [^{18}F]MK-9470 PET data in the human brain. When using compartmental modelling, only K_1 and the model macro parameters (V_T, $V_{ND}k_3$ and K_i) could be identified. It was not possible to estimate k_2 and k_3 reliably in any brain region.

[^{18}F]MK-9470 brain kinetics could be described satisfactorily using a reversible two-tissue model provided that

Table 4 Normalized CBF and [^{18}F]MK-9470 K_1, K_i and FUR values in primary visual areas

Subject	nCBF (%)		K_1 (ml/cm^3/min)		K_i (ml/cm^3/min)		FUR (min^{-1})	
	Video watching	Control	Video watching	Control	Video watching	Control	Video watching	Control
1	117	111	0.040	0.037	0.022	0.023	0.023	0.024
2	151	125	0.018	0.034	0.010	0.010	0.011	0.011
3	137	120	0.023	0.031	0.013	0.012	0.014	0.013
4	148	111	0.022	0.040	0.013	0.013	0.014	0.015
5	141	124	0.022	0.021	0.009	0.009	0.011	0.010
6	135	113	0.053	0.035	0.017	0.015	0.018	0.017

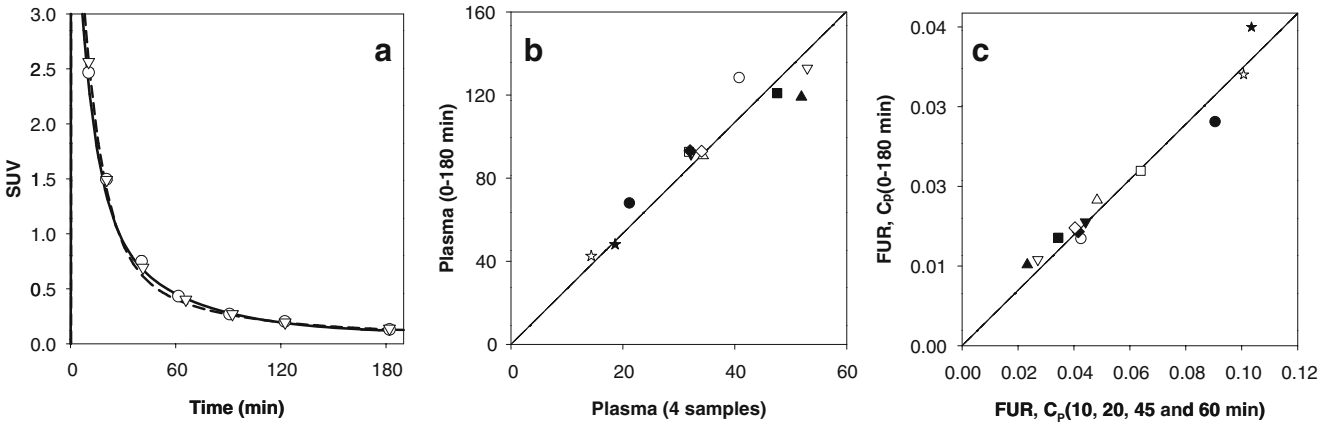

Fig. 9 [^{18}F]MK-9470 plasma kinetics estimation using few blood samples. **a** [^{18}F]MK-9470 plasma concentration in arterial samples (*lines*) and venous samples (*symbols*) from two subjects (average of two measurements). The *solid line* and *circles* represent data from the first subject, the *dashed line* and *triangles* data from the second subject. **b** The integral of the tracer arterial input function from the time of injection to 180 min plotted against the area under the plasma curve using only four samples at 10, 20, 45 and 60 min (r^2=0.88). The integral is on average 2.7 times smaller when using the four data points than when using the curve up to 180 min. **c** Relationship between FUR values in the putamen calculated using the [^{18}F]MK-9470 plasma curve integral from the time of injection to 180 min and FUR values calculated with the area under the plasma curve using only four samples at 10, 20, 45 and 60 min (r^2=0.96). The *solid line* shows to the linear regression between the parameters for all subjects together (slope 0.35, intercept set to zero); *symbols* represent the individual subject values (average of two measurements for ten subjects scanned in two different days)

the rate constant k_4 was fixed throughout the brain. This assumption is reasonable and permitted reliable estimation of k_4 for data acquired over at least 360 min. With this approach, CB1R availability can be assessed using V_T or $V_{ND}k_3$. Furthermore, our results suggest that a 180-min scan could be used to estimate CB1R availability when using a population based k_4 value. The small k_4 value (0.004± 0.001 min^{-1}, six scans) and thus the slow tracer kinetics supported the use of irreversible models to describe the [^{18}F]MK-9470 brain kinetics. A data-driven method with a single trap was better than an irreversible compartment model. This approach permitted estimation of K_i, K_1 and V_B, and no assumptions about time to equilibrium were necessary.

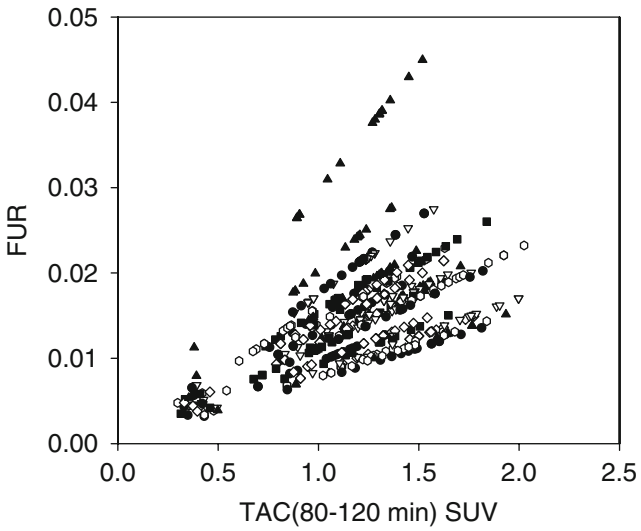

Fig. 10 Relationship between [^{18}F]MK-9470 FUR values estimated using a scan length of 120 min and total tracer concentration in tissue (80–120 min) expressed in SUV for all the subjects in the study. The *symbols* represent data for the individual subjects (average parameters for the subjects receiving two scans in panels 1 and 2)

K_1 values varied between 0.01 and 0.045 ml/g/min in gray matter regions. For a typical CBF value of 0.5 ml/min/ml, the extraction of [^{18}F]MK-9470 was about 9% and the permeability/surface product PS values were in the same range as K_1, suggesting that K_1 is independent of perfusion changes. The data from the visual activation study confirmed that tracer uptake is not flow-limited and thus the fractional uptake ratio can be estimated independently of blood flow changes. The linear relationship between K_i and $V_{T\text{-}2C}$ or $V_{ND}k_3$ values demonstrated that the net irreversible uptake rate constant from plasma and thus FUR values provide CB1R availability information. Furthermore, changes in receptor availability will result in similar changes in brain uptake (90 to 120 min after tracer administration) due to the linear relationship between FUR values and tracer brain uptake (Eq. 3). As shown for [^{11}C]MePPEP [27], the use of the tracer brain uptake can lead to increased sensitivity and precision, so that fewer study samples are required for intergroup comparisons, but at the cost of decreased accuracy due to the lack of correction for the tracer plasma concentration in the case of [^{18}F]MK-9470. In contrast to [^{18}F]MK-9470, the brain uptake of the CB1R tracers [^{11}C]MePPEP [27] and [^{18}F]FMPEP-d_2 [29] underestimates both increases and decreases in receptor density.

Besides being able to reduce the actual scanning period to 30 or 60 min starting 90 to 120 min after [^{18}F]MK-9470 injection, we demonstrated that the blood sampling required to obtain the tracer plasma information can be limited to the first 60 min following tracer injection or even reduced to four blood samples (10, 20, 45 and 60 min). Using a shorter curve or just a few samples introduces a bias in the FUR values. Nevertheless, if the same time interval is used to estimate the tracer plasma data, the bias is consistent between subjects. These results suggest that the FUR value estimated with the modified plasma curve can be used as a surrogate for estimating CB1R availability. Although we have limited data (four scans) showing that both total plasma activity and the fraction of intact [^{18}F]MK-9470 in the plasma are very similar in arterial and venous samples, our results suggest that the burden on the subjects can be further reduced by using a few venous measurements to calculate CB1R availability indexes.

[^{18}F]MK-9470 has been used in human brain for measuring CB1R occupancy by taranabant (MK-0364), a structurally novel acyclic CB1R inverse agonist [7, 13]. The metabolism of [^{18}F]MK-9470 was not affected by the drug and the resulting plasma concentration at baseline and after dosing was similar (assessed in arterial or venous samples). Therefore, it was possible to further simplify the analysis of these studies by calculating TAC_T using the data between 120 and 180 min as an index of CB1R availability. Nevertheless, when performing between-subject comparisons, K_i or FUR values can account for potential differences in tracer plasma kinetics.

The measurement of the plasma input function could be completely avoided by using a reference region in the brain to account for differences in tracer plasma kinetics. However, CB1R is highly expressed throughout the human brain and there is no region that can be used as reference tissue. Although low receptor availability has been reported in the pons [30] and white matter [8, 9], significant decreases in tracer binding have been observed in both regions during studies of CB1R occupancy by taranabant [13].

All currently available tracers for CB1R have high lipophilicity [11] and tend to display high protein binding (>99%), and thus only a small fraction is available to cross the blood–brain barrier. For example, the plasma protein binding of [^{11}C]MePEPP in nonhuman primates has been reported to be >99.9% [11]. In contrast, the free fraction of [^{18}F]MK-9470 in plasma was relatively high (3–6%) with a low variability of the measurements (<2% in three subjects). These data suggest that the large between-subject variability observed for both reversible and irreversible CB1R density indexes using [^{18}F]MK-9470 is due to actual physiological differences in CB1R expression between subjects [15], and not to changes in the free fraction of the tracer in plasma.

In conclusion, we successfully characterized the kinetics of the CB1R inverse agonist [^{18}F]MK-9470 in the human brain. [^{18}F]MK-9470-specific binding in tissue can be quantified accurately using a simplified method. The calculation of FUR values is trivial and the generation of parametric images of CB1R availability is straightforward. Furthermore, the burden on patients can be significantly reduced with the use of a simplified experimental protocol requiring only a 30 to 60-min scanning session and a few venous samples.

Acknowledgments The authors would like to thank Tom Muylle and Dr. Patrick Dupont for their helpful suggestions.

Conflicts of interest S.M.S.B., T.G.H. and I.D.L. are employees of Merck Inc., Co.

H.D.B. is a consultant to Merck Inc., Co.

References

1. Matsuda LA, Lolait SJ, Brownstein MJ, Young AC, Bonner TI. Structure of a cannabinoid receptor and functional expression of the cloned cDNA. Nature 1990;346:561–4.
2. Munro S, Thomas KL, Abu-Shaar M. Molecular characterization of a peripheral receptor for cannabinoids. Nature 1993;365:61–5.
3. Howlett AC, Barth F, Bonner TI, Cabral G, Casellas P, Devane WA, et al. International Union of Pharmacology. XXVII. Classification of cannabinoid receptors. Pharmacol Rev 2002;54:161–202.
4. Katona I, Freund TF. Endocannabinoid signaling as a synaptic circuit breaker in neurological disease. Nat Med 2008;14:923–30.
5. Di Marzo V, Bifulco M, De Petrocellis L. The endocannabinoid system and its therapeutic exploitation. Nat Rev Drug Discov 2004;3:771–84.
6. Van Gaal LF, Rissanen AM, Scheen AJ, Ziegler O, Rossner S. Effects of the cannabinoid-1 receptor blocker rimonabant on weight reduction and cardiovascular risk factors in overweight patients: 1-year experience from the RIO-Europe study. Lancet 2005;365:1389–97.
7. Addy C, Wright H, Van Laere K, Gantz I, Erondu N, Musser BJ, et al. The acyclic CB1R inverse agonist taranabant mediates weight loss by increasing energy expenditure and decreasing caloric intake. Cell Metab 2008;7:68–78.
8. Eggan SM, Lewis DA. Immunocytochemical distribution of the cannabinoid CB1 receptor in the primate neocortex: a regional and laminar analysis. Cereb Cortex 2007;17:175–91.
9. Herkenham M, Lynn AB, Little MD, Johnson MR, Melvin LS, de Costa BR, et al. Cannabinoid receptor localization in brain. Proc Natl Acad Sci U S A 1990;87:1932–6.
10. Grimsey NL, Goodfellow CE, Scotter EL, Dowie MJ, Glass M, Graham ES. Specific detection of CB1 receptors; cannabinoid CB1 receptor antibodies are not all created equal! J Neurosci Methods 2008;171:78–86.
11. Horti AG, Van Laere K. Development of radioligands for in vivo imaging of type 1 cannabinoid receptors (CB1) in human brain. Curr Pharm Des 2008;14:3363–83.
12. Liu P, Lin LS, Hamill TG, Jewell JP, Lanza TJ Jr, Gibson RE, et al. Discovery of N-{(1S,2S)-2-(3-cyanophenyl)- 3-[4-(2-[18F] fluoroethoxy)phenyl]-1-methylpropyl}- 2-methyl-2-[(5-methyl-pyridin-2-yl)oxy]propanamide, a cannabinoid-1 receptor positron emission tomography tracer suitable for clinical use. J Med Chem 2007;50:3427–30.

13. Burns HD, Van Laere K, Sanabria-Bohorquez S, Hamill TG, Bormans G, Eng WS, et al. [18F]MK-9470, a positron emission tomography (PET) tracer for in vivo human PET brain imaging of the cannabinoid-1 receptor. Proc Natl Acad Sci U S A 2007;104:9800–5.
14. Van Laere K, Koole M, Sanabria Bohórquez SM, Goffin K, Guenther I, Belanger MJ, et al. Whole-body biodistribution and radiation dosimetry of the human cannabinoid type-1 receptor ligand 18F-MK-9470 in healthy subjects. J Nucl Med 2008;49:439–45.
15. Van Laere K, Goffin K, Casteels C, Dupont P, Mortelmans L, de Hoon J, et al. Gender-dependent increases with healthy aging of the human cerebral cannabinoid-type 1 receptor binding using [(18)F]MK-9470 PET. Neuroimage 2008;39:1533–41.
16. Hudson HM, Larkin RS. Accelerated image reconstruction using ordered subsets of projection data. IEEE Trans Med Imaging 1994;13:601–9.
17. Zubieta JK, Heitzeg MM, Xu Y, Koeppe RA, Ni L, Guthrie S, et al. Regional cerebral blood flow responses to smoking in tobacco smokers after overnight abstinence. Am J Psychiatry 2005;162:567–77.
18. Vandenberghe J, Dupont P, Van Oudenhove L, Bormans G, Demyttenaere K, Fischler B, et al. Regional cerebral blood flow during gastric balloon distention in functional dyspepsia. Gastroenterology 2007;132:1684–93.
19. Innis RB, Carson R. Consensus nomenclature: its time has come. Eur J Nucl Med Mol Imaging 2007;34:1239.
20. Sanabria-Bohórquez SM, Maes A, Dupont P, Bormans G, de Groot T, Coimbra A, et al. Image-derived input function for [11C] flumazenil kinetic analysis in human brain. Mol Imaging Biol 2003;5:72–8.
21. Delforge J, Syrota A, Mazoyer BM. Identifiability analysis and parameter identification of an in vivo ligand-receptor model from PET data. IEEE Trans Biomed Eng 1990;37:653–61.
22. Gunn RN, Gunn SR, Cunningham VJ. Positron emission tomography compartmental models. J Cereb Blood Flow Metab 2001;21:635–52.
23. Cunningham VJ, Jones T. Spectral analysis of dynamic PET studies. J Cereb Blood Flow Metab 1993;13:15–23.
24. Ishizu K, Nishizawa S, Yonekura Y, Sadato N, Magata Y, Tamaki N, et al. Effects of hyperglycemia on FDG uptake in human brain and glioma. J Nucl Med 1994;35:1104–9.
25. Thie JA. Clarification of a fractional uptake concept. J Nucl Med 1995;36:711–2.
26. Logan J. Graphical analysis of PET data applied to reversible and irreversible tracers. Nucl Med Biol 2000;27:661–70.
27. Terry GE, Liow J, Zoghbi SS, Hirvonen J, Farris AG, Lerner A, et al. Quantitation of cannabinoid CB1 receptors in healthy human brain using positron emission tomography and an inverse agonist radioligand. Neuroimage 2009;48:362–70.
28. Fowler JS, Wang GJ, Logan J, Xie S, Volkow ND, MacGregor RR, et al. Selective reduction of radiotracer trapping by deuterium substitution: comparison of carbon-11-L-deprenyl and carbon-11-deprenyl-D2 for MAO B mapping. J Nucl Med 1995;36:1255–62.
29. Terry GE, Hiervonen J, Liow JS, Zoghbi SS, Gladding R, Tauscher JT, et al. Imaging and quantification of cannabinoid CB1 receptors in human and monkey brain using 18F-labeled inverse agonist radioligands. J Nucl Med 2009;in press.
30. Glass M, Dragunow M, Faull RL. Cannabinoid receptors in the human brain: a detailed anatomical and quantitative autoradiographic study in the fetal, neonatal and adult human brain. Neuroscience 1997;77:299–318.